ACCOUNTS
of chemical research

Monodisperse Magnetic Nanoparticles for Theranostic Applications

DON HO, XIAOLIAN SUN, AND SHOUHENG SUN*

Department of Chemistry, Brown University, Providence, Rhode Island 02912, United States

RECEIVED ON MARCH 22, 2011

CONSPECTUS

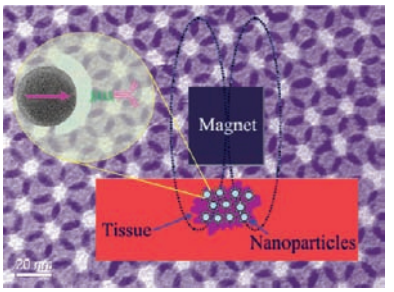

Effective medical care requires the concurrent monitoring of medical treatment. The combination of imaging and therapeutics allows a large degree of control over the treatment efficacy and is now commonly referred to as "theranostics". Magnetic nanoparticles (NPs) provide a unique nanoplatform for theranostic applications because of their biocompatibility, their responses to the external magnetic field, and their sizes which are comparable to that of functional biomolecules. Recent studies of magnetic NPs for both imaging and therapeutic applications have led to greater control over size, surface functionalization, magnetic properties, and specific binding capabilities of the NPs. The combination of the deep tissue penetration of the magnetic field and the ability of magnetic NPs to enhance magnetic resonance imaging sensitivity and magnetic heating efficiency makes magnetic NPs promising candidates for successful future theranostics.

In this Account, we review recent advances in the synthesis of magnetic NPs for biomedical applications such as magnetic resonance imaging (MRI) and magnetic fluid hyperthermia (MFH). Our focus is on iron oxide (Fe_3O_4) NPs, gold-iron oxide (Au−Fe_3O_4) NPs, metallic iron (Fe) NPs, and Fe-based alloy NPs, such as iron-cobalt (FeCo) and iron-platinum (FePt) NPs. Because of the ease of fabrication and their approved clinical usage, Fe_3O_4 NPs with controlled sizes and surface chemistry have been studied extensively for MRI and MFH applications. Porous hollow Fe_3O_4 NPs are expected to have similar magnetic, chemical, and biological properties as the solid Fe_3O_4 NPs, and their structures offer the additional opportunity to store and release drugs at a target. The Au−Fe_3O_4 NPs combine both magnetically active Fe_3O_4 and optically active Au within one nanostructure and are a promising NP platform for multimodal imaging and therapeutics. Metallic Fe and FeCo NPs offer the opportunity for probes with even higher magnetizations. However, metallic NPs are normally very reactive and are subject to fast oxidation in biological solutions. Once they are coated with a layer of polycrystalline Fe_3O_4 or a graphitic shell, these metallic NPs are more stable and provide better contrast for MRI and more effective heating for MFH. FePt NPs are chemically more stable than Fe and FeCo NPs and have shown great potential as contrast agents for both MRI and X-ray computed tomography (CT) and as robust probes for controlled heating in MFH.

1. Introduction

The development of highly effective medicine requires continuous and timely monitoring of the medical treatment process. This combination of monitoring (also called imaging or diagnostics) and therapeutics allows a large degree of control on the treatment efficacy in different individuals and is now commonly referred to as "theranostics".[1] Due to the presence of large percentage of surface atoms, inorganic nanoparticles (NPs), especially those in the dimension <20 nm, have unique physical and chemical properties that are not observed in their bulk forms.[2] This, plus their comparable sizes to biomolecules, makes inorganic NPs ideal functional probes for simultaneous imaging and therapeutic (theranostic) applications. Among various NPs studied

Published on the Web 06/10/2011 www.pubs.acs.org/accounts
10.1021/ar200090c

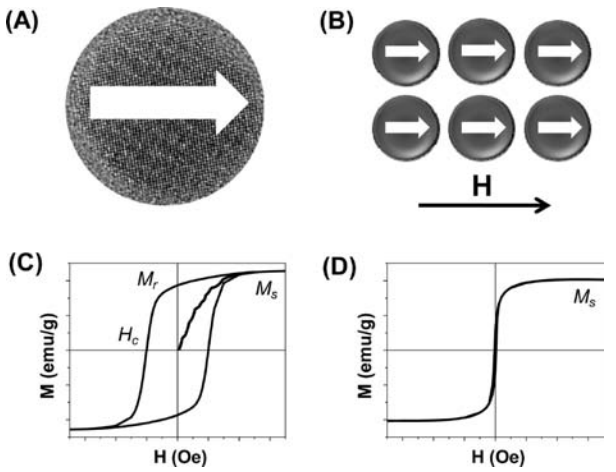

FIGURE 1. Schematic illustration of (A) a single domain magnetic NP with its magnetization pointing to one direction, (B) a group of single domain magnetic NPs aligned along a magnetic field direction, (C) the hysteresis loop of a group of ferromagnetic NPs, and (D) the hysteresis loop of a group of superparamagnetic NPs.

thus far, magnetic NPs containing ferromagnetic iron (Fe) and cobalt (Co) as well as their alloys and oxides have been proven to be the most promising probes for theranostics with the desired imaging sensitivity and therapeutic efficacy.[3−6]

A ferromagnetic NP at the size smaller than 20 nm often contains a single magnetic domain with one collective magnetization direction (Figure 1A).[7] Once these NPs are placed in an external magnetic field (*H*), their magnetization directions can be aligned along the field direction to achieve magnetic saturation with overall magnetization reaching M_s (Figure 1B and C). The ease at which a NP can be aligned is measured by its susceptibility (*M*/*H*). Reduction of the field strength leads to a certain degree of decrease in *M* due to magnetic relaxations, but NPs tend to retain their magnetization direction and have a remnant magnetization (M_r) at zero field strength. To demagnetize these NPs, the external magnetic field must be applied in the opposite direction. The field strength required to demagnetize these NPs is defined as coercivity (H_c) (Figure 1C). When the size of a ferromagnetic NP is reduced to a level where the thermal energy is comparable to the magnetic anisotropy energy, this NP is magnetically unstable and is said to be superparamagnetic.[8] A group of superparamagnetic NPs can be easily magnetized (with large susceptibility) to reach M_s, but they have no H_c and M_r (Figure 1D). Magnetic NPs in the superparamagnetic state have much weaker magnetic dipole interactions and therefore are readily stabilized and dispersed in liquid media.

The diagnostic applications of magnetic NPs are realized in magnetic resonance imaging (MRI).[9] The technique is based on the difference in nuclear magnetic relaxations of the water protons in biological solutions and around solid tissues. A contrast agent modifies the nuclear magnetic relaxation rate of its surrounding protons and changes the signal contrast. Its contrast enhancement effect is measured by the relaxation rate, $R = 1/T$ (s^{-1}) and the relaxivity, $r = R/$concentration ($mM^{-1} \cdot s^{-1}$). The higher relaxivity corresponds to a better contrast effect. Complexes of paramagnetic metal ions (such as Gd^{3+}) serve as a T_1 contrast agent,[10] while magnetic NPs are generally used as a T_2 contrast agent. Their relaxation rate and relaxivity are dependent on $(M_sV)^2$ and d^{-6}, with *V* being the NP volume and *d* the distance between the magnetic core and the surrounding protons.[11] To have better contrast effect, magnetic NPs should have high magnetization (M_s), large volume (*V*), and thin coating (small *d*). However, for biological imaging applications, the hydrodynamic size of a NP is better controlled to be below 50 nm in order for NPs to have long circulation time and to avoid nonspecific uptake.[12] Therefore, magnetic NPs with high magnetization and thin coating are often pursued for sensitive MRI.

Under a fast switching magnetic field, a group of superparamagnetic NPs can become ferromagnetic with their magnetization direction switching quickly along the field directions. The frictions caused by the physical rotation of a NP, Brownian relaxation, and the magnetization reversal within the NP, Neel relaxation, lead to the loss of magnetic energy and the generation of thermal energy. The heating power of these NPs is directly related to *Af*, where *A* is the ferromagnetic hysteresis area and *f* is the frequency of the alternating magnetic field.[13] Used for cancer therapy, this magnetic heating technique has long been known as magnetic fluid hyperthermia (MFH).[14,15] To maximize the NP heating power, the hysteresis area *A* must be as large as possible. However, hyperthermia limitations require that the product $H_{max}f$ should be below 5×10^9 $A \cdot m^{-1} \cdot s^{-1}$ with *f* being above 50 kHz.[14] To ensure optimum MFH effect under the common hyperthermia conditions, magnetic NPs should have small H_c, large susceptibility, and high M_s. The NP heating efficiency is measured by the specific absorption rate (SAR, $W \cdot g^{-1}$). For practical therapeutic applications with minimized side effects, it is critically important to obtain optimum heating efficiency to reach the desired hyperthermia temperature at 41−46 °C, not thermoablation at greater than 50 °C.

2. Chemical Synthesis of Magnetic NPs

To succeed in theranostic applications, magnetic NPs should first be made monodisperse. They should have high magnetization and large susceptibility. They should also be small with a

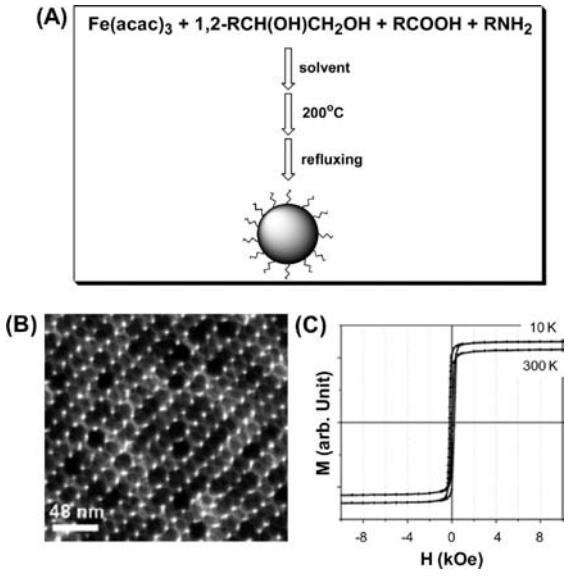

FIGURE 2. (A) Schematic illustration of the chemical synthesis of Fe_3O_4 NPs, (B) TEM image of a 16 nm Fe_3O_4 NP assembly, and (C) Hysteresis loops of the 16 nm Fe_3O_4 NP assembly measured at 10 and 300 K. (A,C) Reprinted with permission from ref 21. Copyright 2002 American Chemical Society. (B) Reprinted with permission from ref 20. Copyright 2004 American Chemical Society.

hydrodynamic size < 50 nm to have extravasation ability and to be stable against uptake by the reticuloendothelial system (RES).[16] Among various magnetic NPs studied, iron oxide, Fe, as well as FeCo and FePt NPs are especially attractive for imaging and therapeutic applications.

2.1. Iron Oxide NPs. Magnetite (Fe_3O_4) and ferrite MFe_2O_4 (M = Mn, Zn) NPs are often selected for biomedical applications due to their chemical/magnetic stability and low cytotoxicity.[17] In the bulk form, these materials are ferrimagnetic due to the antiferromagnetic coupling among Fe(III) in their inverse spinel structure.[18] However, this antiferromagnetic coupling may be eliminated in nanoscale as demonstrated recently by higher magnetizations observed in the $ZnFe_2O_4$ NPs.[19] In general, iron oxide NPs smaller than 20 nm are superparamagnetic at room temperature and have mass magnetizations below their room temperature bulk values at 92 emu·g^{-1} for Fe_3O_4 and 80 emu·g^{-1} for $MnFe_2O_4$.

Monodisperse Fe_3O_4 NPs are often made by reductive decomposition of metal acetylacetonate (acac) in a high temperature organic solution phase.[20−22] In one synthesis, $Fe(acac)_3$ is dissolved in diphenyl either in the presence of 1,2-hexadecanediol, oleic acid, and oleylamine (Figure 2A). 1,2-Hexadecanediol functions as an organic reducing agent to facilitate the formation of Fe_3O_4. Oleic acid and oleylamine are used as surfactants. The step heating at 200 and 265 °C is applied to control Fe_3O_4 nucleation at 200 °C and growth at 265 °C. This synthesis gives 4 nm Fe_3O_4 NPs. With benzyl ether as a solvent and heating temperature raised to 300 °C, 6 nm Fe_3O_4 NPs are obtained. The small Fe_3O_4 NPs can serve as seeds and larger Fe_3O_4 NPs can be made via the seed-mediated growth of Fe_3O_4 in the reductive decomposition of $Fe(acac)_3$. Figure 2B shows the typical transmission electron microscopy (TEM) image of an assembly of 16 nm Fe_3O_4 NPs. Hysteresis loops of the 16 nm Fe_3O_4 NPs measured at both 10 K and at room temperature show that the NPs are ferrimagnetic at 10 K (H_c = 450 Oe) and superparamagnetic at 300 K (M_s = 83 emu·g^{-1}) (Figure 2C).

Iron oleate is another promising precursor used for the synthesis of iron oxide NPs.[23] In this approach, Fe oleate is first prepared from iron chloride ($FeCl_3 \cdot 6H_2O$) and sodium oleate in a mixture solvent of ethanol, water, and hexane at 70 °C. The resulting Fe−oleate complex is then dissolved in a high-boiling-point solvent and then heated to 300 °C to produce monodisperse iron oxide NPs with oleate serving as a surfactant. The synthesis provides a reliable way of making large amount (up to 40 g) of monodisperse NPs with excellent control on NP sizes (tunable from 5 to 22 nm). Monodisperse iron oxide NPs can also be prepared by thermal decomposition of $Fe(CO)_5$ followed by oxidation.[24] By combining decomposition/oxidation of $Fe(CO)_5$ and reductive decomposition of iron oleate complex, the iron oxide NPs can be made with only 1 nm difference in diameter.[25] Recently, ultrasmall Fe_3O_4 NPs ranging from 2.5 to 5 nm are made by thermal decomposition of $Fe(CO)_5$ in benzyl ether at 300 °C followed by room temperature air oxidation.[26] Similar to that in the synthesis of Fe_3O_4 NPs, the high temperature reaction of $Fe(acac)_3$ and $Mn(acac)_2$ gives monodisperse $MnFe_2O_4$ with their size, composition, and shape controlled by the reactant concentrations.[27]

Thermal decomposition of $Fe(CO)_5$ followed by controlled oxidation has been applied to make hollow or porous hollow Fe_3O_4 NPs.[28,29] In this synthesis, amorphous Fe NPs are first made via the decomposition of $Fe(CO)_5$ in the presence of oleylamine. The Fe NPs are exposed to air briefly to form core/shell Fe/Fe_3O_4 NPs with both Fe and Fe_3O_4 in the amorphous state. Controlled oxidation of these core/shell NPs at high temperature (>200 °C) by trimethylamine N-oxide (Me_3NO) yields hollow Fe_3O_4 NPs. In the hollow structure, the Fe_3O_4 shell is polycrystalline. Upon further heating, the Fe_3O_4 crystalline domain is increased, leading to the formation of porous hollow Fe_3O_4 NPs.

2.2. Au−Fe_3O_4 NPs. Dumbbell-like Au−Fe_3O_4 NPs are introduced as one class of multifunctional NPs to control the conjugation of different targeting agents and therapeutic

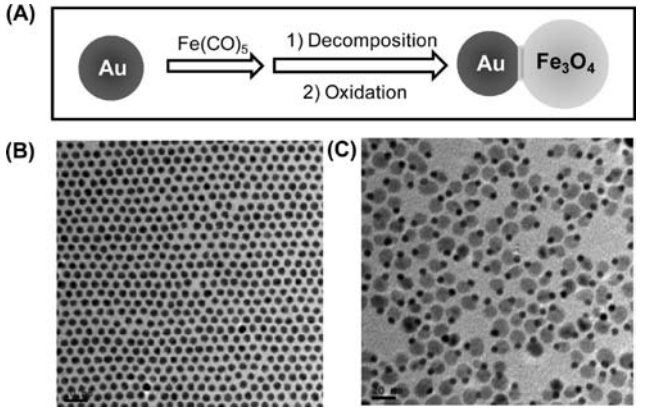

FIGURE 3. (A) Schematic illustration of the growth of Au−Fe_3O_4 NPs. TEM images of the (B) 6 nm Au NPs and (C) 6−17 nm Au−Fe_3O_4 NPs. (A) Reprinted with permission from ref 30. Copyright 2005 American Chemical Society. (B,C) Reprinted with permission from ref 31. Copyright 2009 Wiley.

drugs to the NP surface.[30−32] The Au−Fe_3O_4 NPs are prepared via the decomposition of $Fe(CO)_5$ over the surface of the preformed Au NPs followed by oxidation in air, as illustrated in Figure 3A. The Au NPs can be either synthesized in situ by injecting $HAuCl_4$ solution into the reaction mixture or premade in the presence of oleylamine. More recently, the Au seeding NPs are made by the reduction of $HAuCl_4 \cdot 3H_2O$ with *tert*-butylamine borane complex in 1,2,3,4-tetrahydronaphthalene (tetralin) and oleylamine.[33,34] To synthesize Au−Fe_3O_4 NPs, $Fe(CO)_5$ is injected into 1-octadecene solution containing the Au seeds. Fe nucleates and grows onto Au NPs. Upon exposure to air, the Fe NPs are oxidized to Fe_3O_4 NPs, giving Au−Fe_3O_4 NPs. The size of the Fe_3O_4 NPs is controlled by adjusting the ratio between $Fe(CO)_5$ and Au. Figure 3B and C shows the TEM images of the 6 nm Au seeding NPs and the 6−17 nm Fe_3O_4 NPs. Like Fe_3O_4 NPs, the Au−Fe_3O_4 NPs are also superparamagnetic at room temperature.

2.3. Metallic Fe NPs. Metallic Fe is a typical class of ferromagnetic materials with $M_s = 218$ emu/g Fe. Magnetic NPs of Fe with high magnetizations are important for sensitive MRI and MFH applications. However, metallic Fe NPs are chemically unstable and are oxidized easily to form various iron oxide NPs with much reduced magnetizations.[35] Therefore, one of the biggest challenges in the synthesis is how to stabilize these NPs against fast oxidation.

The common approach to monodisperse Fe NPs is via thermal decomposition of organometallic precursors.[35,36] In a recent synthetic demonstration, monodisperse Fe NPs are made by thermal decomposition of $Fe(CO)_5$ in 1-octadecene and oleylamine.[37] To stabilize these Fe NPs, a dense shell of the crystallized Fe_3O_4 is created over the Fe core via controlled

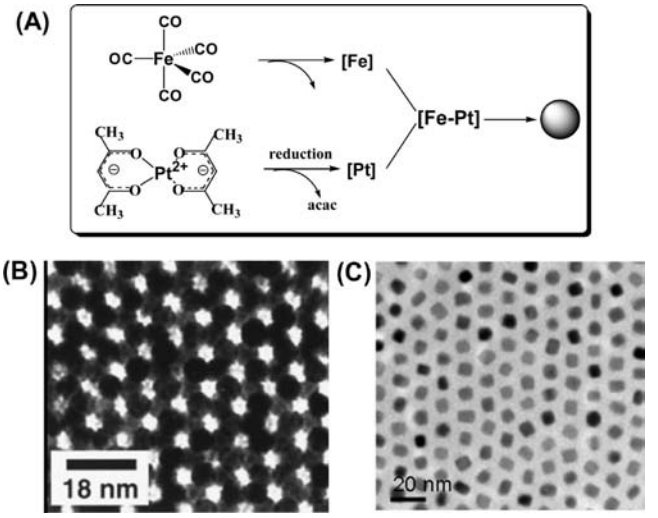

FIGURE 4. (A) Schematic illustration of the formation of FePt NPs from the decomposition of $Fe(CO)_5$ and reduction of $Pt(acac)_2$. TEM images of (B) the 6 nm FePt NPs and (C) the 9 nm FePt NPs. (A) Reprinted with permission from ref 40. Copyright 2006 Wiley. (B) Reprinted with permission from ref 39. Copyright 2000 Science. (C) Reprinted with permission from ref 43. Copyright 2009 American Chemical Society.

oxidation of Fe NPs by $(CH_3)_3NO$. The resultant Fe/Fe_3O_4 NPs show the much enhanced stability after 24 h exposure to air. More recent synthesis shows that body centered cubic (bcc) Fe can be made by the decomposition of $Fe(CO)_5$ in the presence of hexadecylammonium chloride.[38] These bcc-Fe NPs exhibit a drastically increased stability and magnetization and are promising for biomedical applications.

2.4. FePt and FeCo Alloy NPs. FePt and FeCo alloy NPs are two of the most interesting bimetallic NPs studied for biomedical applications. FePt NPs show the structure-dependent magnetic properties from strong ferromagnetism to superparamagnetism and FeCo NPs can offer high magnetization (FeCo has a bulk saturation magnetization of 240 emu/g). FePt NPs are chemically stable against oxidation, but FeCo NPs are chemically unstable and require special treatment for long-term stabilization.

Thermal decomposition of $Fe(CO)_5$ and reduction of $Pt(acac)_2$ in the presence of 1,2-alkanediol is a common way for making monodisperse FePt NPs.[39,40] The synthetic chemistry is illustrated in Figure 4A. Oleic acid and oleylamine are used for FePt NP stabilization. The composition of the FePt NPs is controlled by the $Fe(CO)_5/Pt(acac)_2$ ratio. Figure 4B shows the TEM image of the 6 nm FePt NPs. Fine size tuning on FePt NPs between 2 and 5 nm is achieved by controlling the surfactant to metal ratio.[41] Larger FePt NPs can be made by the decomposition of $Fe(CO)_5$ and reduction of $Pt(acac)_2$ without the presence of 1,2-alkanediol.[42,43] In this synthesis, small Pt-rich FePt NPs are first formed from the

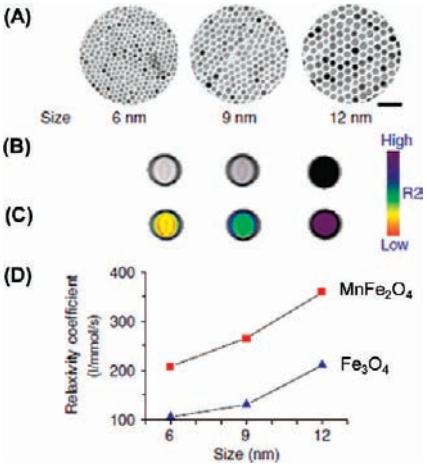

FIGURE 5. (A) TEM images of the $MnFe_2O_4$ NPs (scale bar, 50 nm), (B) T_2-weighted MR images of the corresponding $MnFe_2O_4$ NPs, (C) color maps of the MR images, and (D) plots of NP size versus relaxivity. Reprinted with permission from ref 19. Copyright 2007 Nature.

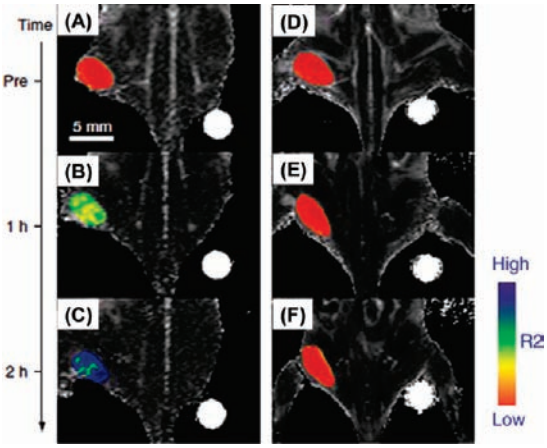

FIGURE 6. Color maps of T_2-weighted MR images of a mouse implanted with the cancer cell line NIH3T6.7 at different time points after injection of the $MnFe_2O_4$–Herceptin (A–C) and the Fe_3O_4–Herceptin (D–F) conjugates. Reprinted with permission from ref 19. Copyright 2007 Nature.

reduction of $Pt(acac)_2$ and the partial decomposition of $Fe(CO)_5$ at temperature < 200 °C. More Fe atoms then coat on the existing Pt-rich FePt NPs, forming larger core/shell NPs. Heating the core/shell structure at 300 °C leads to the Fe diffusion into the Pt-rich core and formation of FePt NPs. Figures 4C shows the TEM image of the 9 nm FePt NPs.

High moment FeCo NPs are synthesized by reductive thermal decomposition of $Fe(CO)_5$ and $Co(\eta^3\text{-}C_8H_{13})(\eta^4\text{-}C_8H_{12})$ or $Co(N(SiMe_3)_2)_2$ in the presence of hexadecylamine and oleic acid,[44] or by interfacial diffusion between Fe and Co in the core/shell Co/Fe structure.[45] As-synthesized NPs have the mass magnetization of up to 200 emu·g^{-1}. FeCo NPs may be better stabilized by a graphitic carbon made by methane chemical vapor deposition at 800 °C.[46] These FeCo/graphitic carbon NPs have been proven to be stable and are promising for sensitive bioimaging applications.

3. Magnetic NPs as Contrast Agent for MRI Applications

Magnetic NPs with controlled magnetizations are promising contrast agents for sensitive MRI applications. This is demonstrated nicely by MFe_2O_4 NPs.[19] These ferrite NPs (6–12 nm) have size-dependent magnetizations with 12 nm $MnFe_2O_4$ and Fe_3O_4 NPs showing the maximum mass magnetization values of 110 and 101 emu·g^{-1} respectively. Once modified with 2,3-dimercaptosuccinic acid and placed in a 1.5 T (T) field, these NPs show the T_2-weighted MR images with the contrast consistent with their magnetization data; larger NPs with higher magnetization generate stronger contrast effect (Figure 5). Due to the thin molecular coating, these NPs have very large relaxivity values, 358 $mM^{-1}\cdot s^{-1}$ for 12 nm $MnFe_2O_4$ NPs and 218 $mM^{-1}\cdot s^{-1}$ for 12 nm Fe_3O_4 NPs.

The cancer detection sensitivity of the ferrite NPs has been evaluated. To perform the test, the NPs are coupled with the cancer-targeting Herceptin, a monoclonal antibody specifically binding to the HER2/neu marker overexpressed on the surface of breast and ovarian cancers.[19] Cell lines with different levels of HER2/neu overexpression are chosen for the study. These are the Bx-PC-3, MDA-MB-231, MCF-7 and NIH3T6.7 with their relative HER2/neu expression levels being 1, 3, 28, and 2300 respectively. The test on the cells incubated with $MnFe_2O_4$–Herceptin indicates that the MR contrast enhancement is related directly to the HER2/neu expression level. In contrast, when stained with the Fe_3O_4–Herceptin, only NIH3T6.7 cells are MR-detectable. Figure 6 shows the color coded MRI of a mouse implanted with the cancer cell line NIH3T6.7 and treated with NP-Herceptin at the dosage of 20 mg/kg. It can be seen that the tumor treated with the $MnFe_2O_4$–Herceptin NPs show color changes from red to blue (Figure 6A–C) but those treated with the Fe_3O_4–Herceptin NPs at the same dosage have no apparent color change (Figure 6D–F).

Ultrasmall Fe_3O_4 NPs (<10 nm in hydrodynamic diameter) are also tested by MRI for tumor-specific targeting. In this demonstration, the 4.5 nm Fe_3O_4 NPs are stabilized by 4-methylcatechol (4-MC).[26] A cyclic arginine-glycine-aspartic acid (cRGD) peptide, c(RGDyK), is coupled to 4-MC via the Mannich reaction (Figure 7A) for integrin targeting. Integrins are a family of cell adhesion molecules consisting of two noncovalently bound transmembrane subunits (α and β), and

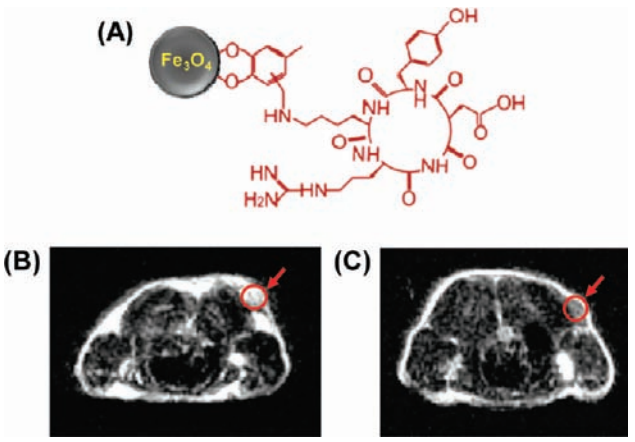

FIGURE 7. (A) Schematic illustration of the coupling of c(RGDyK) peptide to Fe_3O_4 NPs. MRI of the cross section of the U87MG tumors implanted in mice, (B) without NPs and (C) with the injection of 300 μg of c(RGDyK)$-Fe_3O_4$ NPs. Reprinted with permission from ref 26. Copyright 2008 American Chemical Society.

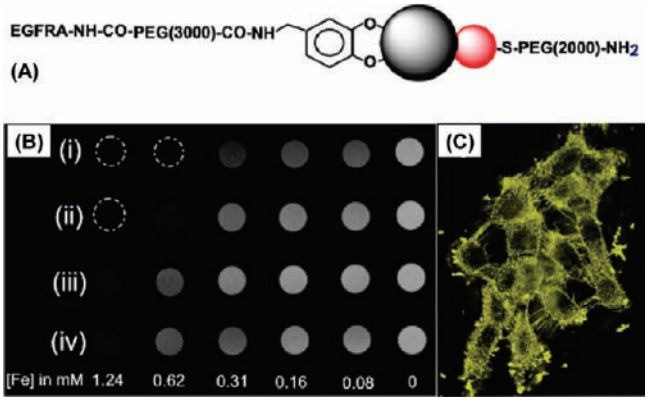

FIGURE 8. (A) Schematic illustration of the surface functionalization of the Au$-Fe_3O_4$ NPs, (B) T_2-weighted MRI of (i) 20 nm Fe_3O_4, (ii) 3–20 nm Au$-Fe_3O_4$, (iii) 8–20 nm Au$-Fe_3O_4$ NPs, and (iv) A431 cells labeled with 8–20 nm Au$-Fe_3O_4$ NPs. (C) Reflection image of the 8–20 nm Au$-Fe_3O_4$ labeled A431 cells. Reprinted with permission from ref 32. Copyright 2008 Wiley.

the integrin $\alpha_v\beta_3$, which binds to RGD-containing components, is significantly upregulated on tumor vasculature and invasive tumor cells. The targeting ability of the c(RGDyK)$-Fe_3O_4$ NPs to integrin $\alpha_v\beta_3$ in vivo is evaluated by T_2-weighted MR imaging with mice bearing U87MG tumors. The r_2 relaxivity of the c(RGDyK)$-Fe_3O_4$ NPs is measured to be 165 $mM^{-1}\cdot s^{-1}$, which is larger than that of the commercial Feridex NPs (104 $mM^{-1}\cdot s^{-1}$) with similar core size. The tumor MR signal intensity decreases by 40% after the injection of c(RGDyK)$-Fe_3O_4$ NP dispersion (Figure 7B and C).

Dumbbell-like Au$-Fe_3O_4$ NPs have been studied as probes for multimodality imaging applications.[32] In this structure, Au NPs are optically active and Fe_3O_4 NPs are magnetically active. The presence of two different NP surfaces within one nanostructure facilitates the controlled functionalization of each NP. Figure 8A illustrates the surface functionalization of the Au$-Fe_3O_4$ NPs. The original oleate/oleylamine coating on Fe_3O_4 is replaced by a catechol unit present in the dopamine molecule that is pre-linked to polyethylene glycol (PEG), and oleylamine around Au is exchanged by HS$-$PEG$-NH_2$ with HS$-$ attaching to Au. The epidermal growth factor receptor antibody (EGFRA) is linked to the PEG via EDC/NHS chemistry on the Fe_3O_4 side. The antibody is used to target A431 human epithelial carcinoma cells that are known to overexpress the epidermal growth factor receptor (EGFR).[47] The preferred binding between EGFR and EGFRA enables the Au$-Fe_3O_4$ to be populated on the surface or within the cytoplasm of A431 cells. MRI analysis reveals that A431 cells labeled with 8–20 nm Au$-Fe_3O_4$ NPs shorten the T_2 relaxation (Figure 8B) with relaxivity $r_2 = 80.4$ $mM^{-1}\cdot s^{-1}$. A431 cells labeled with 8–20 nm Au$-Fe_3O_4$ NPs can also be visualized with a scanning confocal microscope at 594 nm, as shown in Figure 8C. The signal detected is from the Au NPs in the Au$-Fe_3O_4$ structure and reflects the typical morphology of the epithelial cells. The signal is much stronger in the region of cell$-$cell contact due to the preferred binding between EGFR and EGFRA. This Au-NP-based optical probe is very stable and shows no signal loss after 3 days. The detection limit for the 8–20 nm Au$-Fe_3O_4$ NPs is 90 pM Au.

Due to their high magnetizations, metallic NPs should have higher T_2 contrasts than the iron oxide NPs for MRI applications. The oleylamine coated 10 nm/2.5 nm bcc-Fe/Fe_3O_4 NPs are made water-soluble by the addition of an amphiphilic oleylamine-PEG surfactant.[38] Even though these NPs are surrounded by a 15 nm thick coating, the bcc-Fe/Fe_3O_4 NPs still exhibit a r_2 = 220 $mM^{-1}\cdot s^{-1}$, better than the typical iron oxide NP contrast agent Feridex and comparable with the optimized ferrite NPs with 2 nm thick coating.[19] The relaxivity is enhanced even greater for the 7 nm FeCo NPs embedded in a single graphitic shell and functionalized with phospholipid-PEG.[46] Their relaxivity reaches 644 $mM^{-1}\cdot s^{-1}$, nearly 6 times higher than that of the commercial MRI contrast agent Feridex. FePt NPs with sizes from 4 to 12 nm have been studied as MRI contrast agent.[48] In this study, cysteamine is used to replace the original surfactants to make FePt NPs water-soluble. The MRI contrast is NP size-dependent with larger FePt NPs leading to darker images. Due to the high X-ray absorption of Pt (6.95 cm^2/g at 50 keV), these FePt NPs are also promising contrast agent for computed tomography (CT).

4. Magnetic NPs for Therapeutic Applications

The cancer treatment by MFH, based on the sensitivity of cancer cells to heat, has been explored extensively with NPs playing the key role as the local heaters. For 16 nm iron oxide NPs at the superparamagnetism/ferromagnetism transition stage, a hysteresis area $A = 2.3\ mJ \cdot g^{-1}$ with SAR = 1650 $W \cdot g^{-1}$ is observed. However, for the 4 nm NPs, A is reduced to 0.005 $mJ \cdot g^{-1}$ with SAR = 4$W \cdot g^{-1}$.[49] The advantages of using ferrimagnetic/ferromagnetic NPs with high magnetizations to enhance the NP heating efficiency are further demonstrated by 30 nm Fe_3O_4 NPs,[50] as well as by 14.8 nm FeCo NPs and 16.3 nm Fe nanocubes.[51,52] However, these NPs require a strong magnetic field (52 $kA \cdot m^{-1}$) to achieve magnetic saturation. This field strength is far above the safety requirement of 16 $kA \cdot m^{-1}$ for in vivo experiments.[14] The stable weakly ferromagnetic bcc-Fe/Fe_3O_4 NPs have been demonstrated to be efficient for MFH.[38] The heating efficiency of these bcc-Fe/Fe_3O_4 is evaluated in a field with $f = 177$ kHz and $\mu_0 H_{max} = 33$ mT, fulfilling the physiological limitations $H_{max} f < 5 \times 10^9$ $A \cdot m^{-1} \cdot s^{-1}$, and $f > 50$ kHz. Due to their higher magnetization value and small coercive field, the bcc-Fe/Fe_3O_4 NPs have a SAR value of 140 $W \cdot g^{-1}_{Fe}$. This value is comparable with the ferromagnetic 14 nm FeCo NPs[53] and 2 times higher than the best results reported for 20 nm iron oxide NPs.[54]

5. Conclusions

In this Account, we have reviewed the recent advances in synthesizing monodisperse magnetic NPs of iron oxides, Fe, as well as FePt and FeCo for imaging and therapeutic applications. Due to their ease in fabrication and their approved clinical usage, magnetic Fe_3O_4 NPs with controlled sizes and surface chemistry have been studied extensively for MRI and MFH applications. Porous hollow Fe_3O_4 NPs are expected to have similar magnetic, chemical, and biological properties as the solid Fe_3O_4 NPs and have the extra benefits for drug storage and release.[29] The Au−Fe_3O_4 NPs combine both magnetically active Fe_3O_4 and optically active Au within one nanostructure and are a promising NP platform for multimodality imaging and therapeutics.

To achieve even higher sensitivity in MRI and efficacy in MFH, magnetic NPs need to have high magnetizations. This has led to the serious search for metallic Fe and FeCo NPs as new probes. However, metallic NPs are normally very reactive and are difficult to be stabilized against fast/deep oxidation in biological solutions. Recent synthetic progress indicates that, once coated with a layer of polycrystalline Fe_3O_4 or graphitic shell, these metallic NPs can have much enhanced stability and provide indeed better contrast for MRI and more effective heating for MFH.

FePt NPs offer a new nanoplatform for theranostic applications with FePt showing the composition-dependent magnetism. FePt NPs are chemically more stable than Fe and FeCo NPs and are good contrast agents for not only MRI but also CT. The size and composition dependent magnetism also renders FePt NPs a robust probe with controlled magnetic heating power for MFH applications.

Despite exciting progress, previous studies do not provide satisfactory answers to issues on biocirculation, biodistribution, and bioelimination of the magnetic NPs in biological systems. As such issues are related tightly to the interactions between magnetic NPs and biomolecules, understanding NP surface coating and NP interactions with various biological components seems to be necessary. Recent advances in NP synthesis make it possible to study biological properties of magnetic NPs and to develop these NPs into practical probes for theranostic applications.

BIOGRAPHICAL INFORMATION

Don N. Ho earned his B.S. in electrical engineering at the University of Texas (2006) and M.S. in biomedical engineering from Brown University (2008). In 2008, he joined Professor Shouheng Sun's group for his doctoral studies where his current research focuses on inorganic nanoparticle targeting and therapy.

Xiaolian Sun earned her B.S. in the Department of Chemistry, Nanjing University (2008). In 2008, she joined Professor Shouheng Sun`s group for her doctoral studies where her current research focuses on inorganic nanoparticle synthesis and applications.

Shouheng Sun received his Ph.D. in Chemistry from Brown University in 1996. He was a postdoctoral fellow from 1996 to 1998 and a research staff member from 1998 to 2004 at the IBM T. J. Watson Research Center. He moved to Brown University in 2005 and is now a Professor of Chemistry. His research focuses on nanomaterials synthesis and applications in nanomedicine, catalysis, and magnetic energy storage.

The work at Brown University was supported in part by NIH/NCI 1R21CA12859, DOE/EPSCoR DE-FG02-07ER36374, DARPA/ARO W911NF-08-1-0249, and the Brown Imaging Fund.

FOOTNOTES

*To whom correspondence should be addressed. E-mail: ssun@brown.edu.

REFERENCES

1 Warner, S. Diagnostics plus therapy = theranostics. *Scientist* **2004**, *18* (16), 38–39.

2 Murray, C. B.; Kagan, C. R.; Bawendi, M. G. Synthesis and characterization of monodisperse nanocrystals and close-packed nanocrystal assemblies. *Annu. Rev. Mater. Sci.* **2000**, *30*, 545–610.

3 McCarthy, J. R.; Weissleder, R. Multifunctional magnetic nanoparticles for targeted imaging and therapy. *Adv. Drug Delivery Rev.* **2008**, *60* (11), 1241–1251.

4 Kim, J.; Piao, Y.; Hyeon, T. Multifunctional nanostructured materials for multimodal imaging, and simultaneous imaging and therapy. *Chem. Soc. Rev.* **2009**, *38* (2), 372–390.

5 Xie, J.; Huang, J.; Li, X.; Sun, S.; Chen, X. Iron oxide nanoparticle platform for biomedical applications. *Curr. Med. Chem.* **2009**, *16* (10), 1278–1294.

6 Lacroix, L. M.; Ho, D.; Sun, S. H. Magnetic Nanoparticles as Both Imaging Probes and Therapeutic Agents. *Curr. Top. Med. Chem.* **2010**, *10* (12), 1184–1197.

7 Cullity, B. D. *Introduction to Magnetic Materials*; Addison Wesley Publishing Company: Reading, MA, 1972.

8 Unruh, K. M.; Chien, C. L. In *Nanomaterials: Synthesis, Properties and Applications*; Edelstein, A. S., Cammarata, R. C., Eds.; Institute of Physics Publishing: Bristol, U.K., 1996; Ch. 14.

9 Mitchell, D. G. *MRI Principles*; W. B. Saunders Company: Philadelphia, PA, 1999.

10 Caravan, P. Strategies for increasing the sensitivity of gadolinium based MRI contrast agents. *Chem. Soc. Rev.* **2006**, *35*, 512–523.

11 Koenig, S. H.; Kellar, K. E. Theory of 1/T-1 and 1/T-2 Nmrd Profiles of Solutions of Magnetic Nanoparticles. *Magn. Reson. Med.* **1995**, *34* (2), 227–233.

12 Moghimi, S. M.; Hunter, A. C.; Murray, J. C. Long-circulating and target-specific nanoparticles: Theory to practice. *Pharmacol. Rev.* **2001**, *53* (2), 283–318.

13 Lu, J. J.; Hunag, H. L.; Klik, I. Field orientations and sweep rate effects on magnetic switching of Stoner−Wohlfarth particles. *J. Appl. Phys.* **1994**, *76*, 1726–1732.

14 Jordan, A.; Scholz, R.; Wust, P.; Fahling, H.; Felix, R. Magnetic fluid hyperthermia (MFH): Cancer treatment with AC magnetic field induced excitation of biocompatible superparamagnetic nanoparticles. *J. Magn. Magn. Mater.* **1999**, *201*, 413–419.

15 Moroz, P.; Jones, S. K.; Gray, B. N. Magnetically mediated hyperthermia: current status and future directions. *Int. J. Hyperthermia* **2002**, *18* (4), 267–284.

16 Xie, J.; Xu, C.; Kohler, N.; Hou, Y.; Sun, S. Controlled PEGylation of monodisperse Fe3O4 nanoparticles for reduced non-specific uptake by macrophage cells. *Adv. Mater.* **2007**, *19* (20), 3163–3166.

17 Lewinski, N.; Colvin, V.; Drezek, R. Cytotoxicity of nanoparticles. *Small* **2008**, *4* (1), 26–49.

18 O'Handley, R. C. *Modern Magnetic Materials-Principles and Applications*; John Wiley & Sons: New York, 2000; pp 126−132.

19 Lee, J.-H.; Huh, Y.-M.; Jun, Y.-w.; Seo, J.-W.; Jang, J.-t.; Song, H.-T.; Kim, S.; Cho, E.-J.; Yoon, H.-G.; Suh, J.-S.; Cheon, J. Artificially engineered magnetic nanoparticles for ultra-sensitive molecular imaging. *Nat. Med.* **2007**, *13* (1), 95–99.

20 Sun, S. H.; Zeng, H. Size-controlled synthesis of magnetite nanoparticies. *J. Am. Chem. Soc.* **2002**, *124* (28), 8204–8205.

21 Sun, S. H.; Zeng, H.; Robinson, D. B.; Raoux, S.; Rice, P. M.; Wang, S. X.; Li, G. X. Monodisperse MFe2O4 (M = Fe, Co, Mn) nanoparticles. *J. Am. Chem. Soc.* **2004**, *126* (1), 273–279.

22 Niederberger, M. Nonaqueous Sol−Gel Routes to Metal Oxide Nanoparticles. *Acc. Chem. Res.* **2007**, *40* (9), 793–800.

23 Park, J.; An, K. J.; Hwang, Y. S.; Park, J. G.; Noh, H. J.; Kim, J. Y.; Park, J. H.; Hwang, N. M.; Hyeon, T. Ultra-large-scale syntheses of monodisperse nanocrystals. *Nat. Mater.* **2004**, *3* (12), 891–895.

24 Hyeon, T.; Lee, S. S.; Park, J.; Chung, Y.; Na, H. B. Synthesis of Highly Crystalline and Monodisperse Maghemite Nanocrystallites without a Size-Selection Process. *J. Am. Chem. Soc.* **2001**, *123* (51), 12798–12801.

25 Park, J.; Lee, E.; Hwang, N. M.; Kang, M. S.; Kim, S. C.; Hwang, Y.; Park, J. G.; Noh, H. J.; Kini, J. Y.; Park, J. H.; Hyeon, T. One-nanometer-scale size-controlled synthesis of monodisperse magnetic iron oxide nanoparticles. *Angew. Chem., Int. Ed.* **2005**, *44* (19), 2872–2877.

26 Xie, J.; Chen, K.; Lee, H. Y.; Xu, C. J.; Hsu, A. R.; Peng, S.; Chen, X. Y.; Sun, S. H. Ultrasmall c(RGDyK)-coated Fe_3O_4 nanoparticles and their specific targeting to integrin alpha(v)-beta(3)-rich tumor cells. *J. Am. Chem. Soc.* **2008**, *130* (24), 7542–7543.

27 Zeng, H.; Rice, P. M.; Wang, S. X.; Sun, S. H. Shape-controlled synthesis and shape-induced texture of $MnFe_2O_4$ nanoparticles. *J. Am. Chem. Soc.* **2004**, *126* (37), 11458–11459.

28 Peng, S.; Sun, S. H. Synthesis and characterization of monodisperse hollow Fe3O4 nanoparticles. *Angew. Chem., Int. Ed.* **2007**, *46* (22), 4155–4158.

29 Cheng, K.; Peng, S.; Xu, C. J.; Sun, S. H. Porous Hollow Fe_3O_4 Nanoparticles for Targeted Delivery and Controlled Release of Cisplatin. *J. Am. Chem. Soc.* **2009**, *131* (30), 10637–10644.

30 Yu, H.; Chen, M.; Rice, P. M.; Wang, S. X.; White, R. L.; Sun, S. H. Dumbbell-like bifunctional Au-Fe_3O_4 nanoparticles. *Nano. Lett.* **2005**, *5* (2), 379–382.

31 Lee, Y. M.; Garcia, M. A.; Huls, N. A. F.; Sun, S. H. Synthetic Tuning of the Catalytic Properties of Au-Fe_3O_4 Nanoparticles. *Angew. Chem., Int. Ed.* **2010**, *49* (7), 1271–1274.

32 Xu, C.; Xie, J.; Ho, D.; Wang, C.; Kohler, N.; Walsh, E. G.; Morgan, J. R.; Chin, Y. E.; Sun, S. Au-Fe_3O_4 dumbbell nanoparticles as dual-functional probes. *Angew. Chem., Int Ed.* **2008**, *47* (1), 173–176.

33 Peng, S.; Lee, Y. M.; Wang, C.; Yin, H. F.; Dai, S.; Sun, S. H. A Facile Synthesis of Monodisperse Au Nanoparticles and Their Catalysis of CO Oxidation. *Nano Res.* **2008**, *1* (3), 229–234.

34 Lee, Y.; Loew, A.; Sun, S. H. Surface- and Structure-Dependent Catalytic Activity of Au Nanoparticles for Oxygen Reduction Reaction. *Chem. Mater.* **2010**, *22* (3), 755–761.

35 Dumestre, F.; Chaudret, B.; Amiens, C.; Renaud, P.; Fejes, P. Superlattices of iron nanocubes synthesized from Fe[N(SiMe3)(2)](2). *Science* **2004**, *303* (5659), 821–823.

36 Green, M. Organometallic based strategies for metal nanocrystal synthesis. *Chem. Commun.* **2005**, *24*, 3002–3011.

37 Peng, S.; Wang, C.; Xie, J.; Sun, S. H. Synthesis and stabilization of monodisperse Fe nanoparticles. *J. Am. Chem. Soc.* **2006**, *128* (33), 10676–10677.

38 Lacroix, L.-M.; Frey Huls, N.; Ho, D.; Sun, X.; Cheng, K.; Sun, S., Stable Single-Crystalline Body Centered Cubic Fe Nanoparticles. *Nano Lett.* 2011, 10.1021/nl200110t.

39 Sun, S. H.; Murray, C. B.; Weller, D.; Folks, L.; Moser, A. Monodisperse FePt nanoparticles and ferromagnetic FePt nanocrystal superlattices. *Science* **2000**, *287* (5460), 1989–1992.

40 Sun, S. H. Recent advances in chemical synthesis, self-assembly, and applications of FePt nanoparticles. *Adv. Mater.* **2006**, *18* (4), 393–403.

41 Momose, S.; Kodama, H.; Uzumaki, T.; Tanaka, A. Fine tuning of the sizes of FePt nanoparticles. *Jpn. J. Appl. Phys., Part 1* **2005**, *44* (2), 1147–1149.

42 Chen, M.; Liu, J. P.; Sun, S. H. One-step synthesis of FePt nanoparticles with tunable size. *J. Am. Chem. Soc.* **2004**, *126* (27), 8394–8395.

43 Xu, C. J.; Yuan, Z. L.; Kohler, N.; Kim, J. M.; Chung, M. A.; Sun, S. H. FePt Nanoparticles as an Fe Reservoir for Controlled Fe Release and Tumor Inhibition. *J. Am. Chem. Soc.* **2009**, *131* (42), 15346–15351.

44 Desvaux, C.; Amiens, C.; Fejes, P.; Renaud, P.; Respaud, M.; Lecante, P.; Snoeck, E.; Chaudret, B. Multimillimetre-large superlattices of air-stable iron-cobalt nanoparticles. *Nat. Mater.* **2005**, *4* (10), 750–753.

45 Wang, C.; Peng, S.; Lacroix, L. M.; Sun, S. H. Synthesis of High Magnetic Moment CoFe Nanoparticles via Interfacial Diffusion in Core/Shell Structured Co/Fe Nanoparticles. *Nano Res.* **2009**, *2* (5), 380–385.

46 Seo, W. S.; Lee, J. H.; Sun, X. M.; Suzuki, Y.; Mann, D.; Liu, Z.; Terashima, M.; Yang, P. C.; McConnell, M. V.; Nishimura, D. G.; Dai, H. J. FeCo/graphitic-shell nanocrystals as advanced magnetic-resonance-imaging and near-infrared agents. *Nat. Mater.* **2006**, *5* (12), 971–976.

47 Kawamoto, T.; Sato, J. D.; Le, A.; Polikoff, J.; Sato, G. H.; Mendelsohn, J. Growth-Stimulation of A431 Cells by Epidermal Growth-Factor - Identification of High-Affinity Receptors for Epidermal Growth-Factor by an Anti-Receptor Monoclonal-Antibody. *Proc. Natl. Acad. Sci. U.S.A.* **1983**, *80* (5), 1337–1341.

48 Chou, S. W.; Shau, Y. H.; Wu, P. C.; Yang, Y. S.; Shieh, D. B.; Chen, C. C. In Vitro and in Vivo Studies of FePt Nanoparticles for Dual Modal CT/MRI Molecular Imaging. *J. Am. Chem. Soc.* **2010**, *132* (38), 13270–13278.

49 Lacroix, L. M.; Carrey, J.; Respaud, M. A frequency-adjustable electromagnet for hyperthermia measurements on magnetic nanoparticles. *Rev. Sci. Instrum.* **2008**, *79* (9), 093909.

50 Raikher, Y.; Stepanov, V. Dynamic hysteresis of a superparamagnetic nanoparticle at low-to-intermediate frequencies. *J. Magn. Magn. Mater.* **2006**, *300*, e311–e314.

51 Mehdaoui, B.; Meffre, A.; Lacroix, L. M.; Carrey, J.; Lachaize, S.; Gougeon, M.; Respaud, M.; Chaudret, B. Large specific absorption rates in the magnetic hyperthermia properties of metallic iron nanocubes. *J. Magn. Magn. Mater.* **2010**, *322* (19), L49–L52.

52 Pavel, M.; Gradinariu, G.; Stancu, A. Study of the Optimum Dose of Ferromagnetic Nanoparticles Suitable for Cancer Therapy Using MFH. *IEEE Trans. Magn.* **2008**, *44* (11), 3205–3208.

53 Lacroix, L. M.; Malaki, R. B.; Carrey, J.; Lachaize, S.; Respaud, M.; Goya, G. F.; Chaudret, B. Magnetic hyperthermia in single-domain monodisperse FeCo nanoparticles: Evidences for Stoner-Wohlfarth behavior and large losses. *J. Appl. Phys.* **2009**, *105* (2), 023911.

54 Zhang, L. Y.; Gu, H. C.; Wang, X. M. Magnetite ferrofluid with high specific absorption rate for application in hyperthermia. *J. Magn. Magn. Mater.* **2007**, *311* (1), 228–233.